Numerical modeling of the mechanical behavior of proton exchange membrane fuel cell performance: Design of experiment study and optimization

Ghinwa Ouaidat, Abel Cherouat, Raed Kouta, Dominique Chamoret

Numerical modelling of the mechanical behavior of proton exchange membrane fuel cell performance: design of experiment study and optimization

Ghinwa Ouaidat[a,b,*], Abel Cherouat[a], Raed Kouta[b], Dominique Chamoret[c]

a. University of Technology of Troyes-GAMMA3, 12 rue Marie Curie, 10004 Troyes, France
b. University of Technology of Troyes-M2S, 12 rue Marie Curie, 10004 Troyes, France
c. ICB UMR 6303, CNRS, UBFC, University of Technology of Belfort-Montbéliard, 90010 Belfort, France
Ghinwa.ouaidat@utt.fr , abel.cherouat@utt.fr , raed.kouta@utbm.fr, dominique.chamoret@utbm.fr

*: *corresponding author*

Abstract

The fundamental magnitude which can be associated with the performance of a fuel cell is the contact pressure. The contact pressure sustained by the GDL will directly impact the electrical performance of the fuel cell, in particular the contact resistance. This contact resistance can be modeled in two different ways: analytically from the mechanical model and electrically from a mechanical - electrical coupling model. We opted for the analytical resolution. The contact resistance was calculated analytically, based on the mechanical model. Note that the contact resistance is influenced by several mechanical parameters such as the clamping pressure, the porosity of the GDL and the dimensions of two components GDL and BPP. This porosity decreases during compression in order to make waterproofing. In our study, to model the porosity of the GDL, two approaches were presented: pore network approach (used in the case of low porosity) and continuous approach (used in the case of high porosity). It is necessary to quantify and verify the influence of three factors: the porosity of the GDL, the bending radius of the bipolar plate and the thickness of the GDL on the contact pressures. To do this, we conducted two experimental plans on the stack: one corresponding to low porosity and the other one to high porosity. The optimal parameters having been identified, we found a good correlation between the numerical results and the experimental results found in the bibliography.

Keywords: PEMFC, Design of Experiments, Contact Pressure, Electrical Resistance, Clamping pressure

1. Background and Issues

The fuel cell is an energy converter that allows the transformation of the chemical energy contained in the hydrogen into electrical and thermal energy. The different type of fuel cells (AFC, PEMFC, DMFC, PAFC, MCFC and SOFC) are differentiated by the electrolyte, the fuel and the operating conditions [1]. In the last ten years, the biggest development efforts have been focused on the Proton Exchange Membrane Fuel Cell (PEMFC) in the automobile industry in order to allow rapid cold start and increase the performance of the fuel cell at low temperatures (between 30 and 100˚C). A PEMFC is an assembly of cells associated in series of stack constituted of multiple components (ED, BPP, GDL and MEA). These components must be mechanically maintained in order to guarantee perfect waterproofing, adequate gas diffusion and electrical conductivity, thus allowing a better performance of the fuel cell.

The fuel cell is a complex multi-physical system where multiple phenomena are fully coupled: mechanical, electrical, thermal and fluidic [2], [3] and [4]. This performance depends on several different parameters like: thermo-mechanical (temperature and clamping pressure), design (dimension and shape of each component) and material (properties of each component). All these parameters, especially the clamping pressure, can affect the assembly of the components and particularly mechanical parameters such as the contact pressure at the interface of each component. The optimal pressure generates adapted mechanical strain and stresses in the MEA and the GDL and the gas circulation in the MEA and minimizes the contact resistance.

At the component assembling stage, a high clamping pressure provokes irreversible deformations and high mechanical stress in the thin membrane and the flexible GDL, which affects the contact pressure distribution, decreases the porosity and the pore size under the BPP channels, damages the MEA and cracks the bipolar plate… However, a low clamping pressure can cause a leak of gases between the components, which decreases the contact pressure distribution and the electrical power density (see Table 1).

Table 1: Effects of the mechanical parameters on the performance of the Fuel Cell [1], [5], [3] and [6].

	Mechanical parameters	Explanation	Consequence
MEA	Thickness (mm) ($0.051 \leq T_{MEA} \leq 0.183$)	Imbalance in the flow of the ions H+ through the membrane	Reducing the thickness of the membrane reduces its resistance and decreases the ohmic losses
GDL	Thickness (mm) ($0.11 \leq T_{GDL} \leq 0.377$)	Mass transport of the GDL	Reducing the thickness of the GDL increases the mass transport through it and thus reduces the losses of mass transport
	Porosity (%) ($10 \leq \varepsilon \leq 90$)	Mass transport of the GDL	Increasing the porosity of the GDL enhances the mass transport and reduces its losses A weak porosity leads to an insufficient reactive gas circulation: the water produced by the electrochemical reaction won`t be evacuated which leads to a flood in the GDL plate
	Clamping Pressure (MPa) ($0 < P \leq 10$)	Deformation of the GDL and on the contact resistance between the GDL and the bipolar plate	A strong pressure compression reduces the permeability of gases, enhance the conductivity and reduces the contact resistance between the GDL and the bipolar plate and reduces the total losses
BPP	Width of the channel (mm) ($0.5 \leq W_{CN} \leq 4$)	Circulation of reactive gases	A small channel leads to an insufficient supply of reactive gases
	Width of the Rib (mm) ($0.5 \leq W_{Rib} \leq 4$)	Contact surface between the GDL plates and the bipolar plate	A small width of the Rib leads to a high contact resistance at the interface
	Bending radius (mm) ($0.1 \leq R_{RIB} \leq 0.9$)	Contact between the bipolar plate and the GDL	When the bending radius increases, on the one hand, the length of contact between the Bipolar plate and the GDL decreases, which increases contact resistance, but, on the other hand, an increase in contact pressure results in a decrease in resistance.

Many experimental and numerical studies are carried out to optimize the assembly parameters of fuel cells components and improve its performance. Most of the results show a significant impact of the clamping pressure on the sealing, the damage of the thin flexible membrane and the contact pressure GDL/ BPP.

Akiki, T. [6] studied the influence of different geometries of the bipolar plate. Akiki, T. showed that at

a very high pressure, the bipolar plate of graphite with a trapezoidal section and a bending radius of R_{RIB} = 0.2 mm corresponds to the best performance of the fuel cell.

Muthukumar, M. *et al.* [7] studied the influence of the width of the draining channels on the current density. They show that the optimal width of channels of W_{CN} = 0.5mm produce a maximum of power density of 0.44W/cm^2 (V=0.4V). In addition, Kahveci, E. E., & Taymaz, I. [8] have shown that increasing the flow channel width of the bipolar plate from $0.8 \leq W_{CN} \leq 1.2$ mm decreases the gas flow in the GDL and the current density.

Lai, X. *et al.* [9] studied the influence of the variation of the bending radius of the bipolar plate R_{RIB} range from 0.1 to 0.9 mm on the distribution of contact pressure between the GDL/BPP. The results show that increasing the bending radius of the bipolar plate from 0.1 to 0.6 mm results in a decrease in contact resistance from 8.5 to 7.10-3 Ω. Beyond 0.6 mm, the contact resistance begins to increase.

Dey, T. *et al.* [10] studied the effect of End Plates shape and the number of bolt on the distribution of contact pressure. Several geometries were studied numerically (extruded hexagonal, extruded triangles, plain flat) and have shown that the extruded hexagonal geometry presents better distribution of contact pressure all over the contact surface, with a contact resistance per unit surface that varies from R = 0 to 30Ω. For the effect of the number of bolts, this study showed a low contact pressure is observed with four bolts. This contact pressure increases with the number of bolts. Thus, a number of 10 bolts gives a better contact pressure distribution.

Movahedi, M. *et al.* [11] studied the effect of clamping pressure on the cell deformation, especially the GDL and its characteristics: thickness, porosity and permeability. They optimize the range of clamping pressure where the current density and the cell's performance are maximized.

Mason, T. J. *et al.* [12] showed that with a clamping pressure of P = 0.5 MPa, an increase in the mass transport area of the GDL is observed. In addition, Habibnia, M. *et al.* [13] proved that the clamping pressure should be more than P = 2.0 MPa to ensure the full tightness of the assembly.

In the same field, Irmscher, P. *et al.* [14] studied the influence of clamping pressure P for optimum contact pressure with two types of GDL (SGL 29BCE, Toray TGP-H 060 and Freudenberg). The obtained results show that, the SGL 29BCE presents an average pressure of P = 0.5 N/mm^2, however Toray TGP-H 060 and Freudenberg have their optimum in higher-pressure ranges.

Regarding studies on the number of cells, Carral, C. *et al.* [15], Bates, A. *et al.* [16], Zhou, P. *et al.* [17] and Alizadeh, E. *et al.* [18] showed that a better uniformity of contact pressure distribution was

observed for a very high number of cells. For a smaller cell number (2 and 5 cells), a low value of contact pressure is observed (0.1 MPa) causing bad contact. On the other hand, the minimum number of cells is around 16 for better pressure distribution and therefore better electrical performance.

Lai, Xinmin, *et al.* [19] developed a 3D model of a fuel cell and studied the effects of clamping pressure and the position of end plate bolts on the MEA pressure distribution. They used the response surface method (RSM) to establish a relationship between the design variables (the assembly pressure and the bolt position) and the output variables (maximum stress on the membrane and the difference between the stresses maxi and mini) in order to improve and optimize the process. They have shown that the clamping pressure P influences the pressure distribution of MEA more than the bolt position of the end plate and that the maximum stress of the membrane occurs when the assembly pressure and the position of bolts are at their highest level.

Atyabi, Seyed Ali*, et al*. [20] developed a multi-physical 3D model and studied the effect of clamping pressure on the contact resistance between GDL/BPP. The results show that the increase in the clamping pressure leads to a localization of the distribution of electric current in the area located at the corner of the bipolar plate. In addition, this increase in clamping pressure up to 3.5 MPa leads to an increase in the electric potential which will accumulate in the area close to the channel wall, on the other hand above 3.5 MPa, the electrical potential decreases.

Chien, Chi-Hui, *et al.* [21] developed a mechanical thermal model to study the effect of clamping pressure on the contact resistance between GDL/BPP. The increase in the clamping pressure from 1 to 7 MPa leads, on the one hand, to an increase in the stress Von. Mises from 0.668 to 4.475 MPa in the GDL and from 1.684 to 8.470MPa in the BPP and on the other hand, to a decrease in the contact resistance from 59 to 15 mΩ and a decrease in the porosity of 77 up to 72%. Then, they showed that the variation of the conductivity and the porosity as a function of the clamping pressure makes it possible to identify the optimal clamping pressure (4MPa) allowing a better performance of the fuel cell.

García-Salaberri, Pablo A *et al*. [22] studied the inhomogeneous compression effect on the mechanical characteristics of the Troray type GDL. They showed that under an imposed vertical displacement from 0 to 60 mm, the stress is localized under the corner of the rib of the BPP involving a reduction in porosity (about 12% for the largest imposed displacement) under the rib of the bipolar plate, on the other hand an increase in the porosity under the channel since under the channel the GDL undergoes a slight tensile stress. Then, a comparison between the nonlinear orthotropic model

and two linear isotropic models was carried out in order to study the effect of the mechanical behavior of GDL under inhomogeneous compression.

García-Salaberri, P. A. *et al*. [23] studied the effects of compression and channel geometry of BPP on the performance of fuel cell. Two types of BPP channels were studied (serpentine and parallel). They have shown that in the case of parallel geometry channels, the current density is higher under the channel because of the shorter diffusion path required for the methanol molecules to reach the catalyst layer. The performance of the cell is degraded under the rib of BPP due to the local reduction of the effective diffusivity. In the case of serpentine type channels, higher current densities were observed compared to the case of parallel type channels.

Carcadea E *et al*. [24] conduct other studies on the influence of different characteristics of the GDL (thickness, porosity, interfacial resistance between GDL/BPP) on the fuel cell performance. The results show that reducing the thickness of the GDL from T_{GDL} = 350 µm to 250 µm leads to an increase in performance, especially in the two zones of the polarization curve (ohmic polarization and concentration polarization). In addition, the fuel cell performance improves with increasing the GDL porosity range from 40 % ≤ ε ≤ 78%. The highest current density values (1.7 A/cm^2) were those of the case with the highest GDL porosity (ε = 78%).

Vlahinos, A. *et al.* [25] studied the effect of the elasticity modulus of the bipolar plates (E_{BPP} = 5100 MPa), the thickness of the bipolar plate (T_{BPP} = 1.27 mm), the thickness of the membrane (T_{MEA} = 0.457 mm) and the bolt clamping force (100 N) on the pressure distribution. The numerical results have shown that the bipolar plate and the MEA thickness is the most significant factor on the pressure distribution. However, the MEA thickness T_{MEA} and the elastic properties are the most influential input variables on the pressure uniformity of the MEA in the middle of the stack.

Toghyani, S. *et al*. [26] studies have shown that increasing the clamping pressure P decreases the thickness of the GDL, which increases the mass transfer in the GDL and the molar fraction of oxygen in the catalyst layer.

Other experimental and numerical studies [27-35] have shown that:

- The clamping pressure affects the performance of the fuel cell while also affecting the contact resistance (due to the assembling procedure), the porosity of the GDL, as well as the permeability.
- The contact resistance between the GDL and the bipolar plate decreases in a non-linear manner with the increase of the clamping force. Moreover, a uniform distribution of pressure causes a

decrease by 30% of the contact resistance.

- A strong clamping pressure causes an increase of the contact pressure and reduces the performance of the fuel cell.
- A tightening torque of 1.5 Nm corresponds to a better performance of the fuel cell with a uniform distribution of contact pressure between GDL/BPP.
- The contact resistance decreases exponentially under high clamping pressure.

As the GDL is the most sensitive component of the fuel cell, any change in its structure results in a change in its porosity, which strongly influences the performance of the cell. Several studies have shown the influence of the porosity of GDL on the phenomena of mass transport in GDL. In their modeling work, the GDL is modeled as a classical porous medium and the transport phenomena are modeled using classical local equations of the continuous approach of porous media. Consequently, the major problem will be to enquire the transport properties involved in the models. Most of the authors are based on the use of classical relations for these properties, resulting from experiments with media like sand, which are therefore a priori not relevant for fibrous media like GDL. Therefore, the continuous approach presents a more fundamental problem due to the absence of scale separation (measured in pore size, a GDL is only about ten pore size thick). This is the reason why it will be interesting to develop alternative approaches, allowing calculation directly at the scale of the microstructure.

In our case, we will concentrate on the pore network approach. These pores are filled with a fluid or a mixture of fluids. Transport phenomena such as flows, diffusion and conduction in this porous medium and contact phenomena require robust modeling of the geometry of the GDL and precisely its pores. The modeling difficulty is strongly linked to the singular characteristics of the components of the PEMFC (thin thickness of the GDL, pore sizes, radius of curvature of the BPP, etc.).

In this context, we have developed two main approaches to characterize the porosity of GDL: first, we concentrated on the pore networks used in the case of a small variation in porosity (between 10 and 57%). Then we focused our attention on the continuous approach used in the case of a high variation in porosity (between 68 and 88%).

The literature review shows that no studies associated the design of experiment to optimize the fuel cell stack parameters corresponding to a better mechanical and electrical performance. This work aims to understand the influence of the different parameters: geometrical and mechanical on the operating behavior of a fuel cell system from only a mechanical point of view through an experimental plan.

As there are no studies on the influence of the pore dimensions in the GDL on the distribution of the contact pressures between GDL/BPP, we are especially interested in some parameters (porosity of the GDL, thickness of the GDL and bending radius of the BPP) influence the contact pressure. To realize this experimental plan in good conditions and in reasonable timing of calculations (reasonable timing), we associated it with a 2D mechanical finite elements model of a fuel cell.

The subsequent parts of this article are organized as follows: the finite element model using ABAQUS software introduced in section 2 presents the 2D geometry of two half-channel and one rib of the cell, the behavior of each component and the loading conditions. The design of experiment for low porosity and high porosity is presented in section 3. The optimal parameters corresponding to a better performance of the fuel cell stack are used to simulate the behavior of each component under compression loading. Comparison with experimental results is performed to validate the proposed design of experiment approach.

2. Material and method

Fuel cell system electrical performance is very dependent on the contact pressure evolution, in particular, the ohmic losses related to the contact resistance [26], [27] and [36]. To optimize the fuel cell system and to improve its durability, the design of experiments of a simplified fuel cell stack assembly is studied numerically using ABAQUS software [51]. In this section, we will present two approaches to simulate the behavior of the GDL under mechanical compression loading and the contact resistance between several stack components.

2.1 Finite Element Model

Due to the geometrical symmetry of the cell, the isotropic isothermal behavior and the loading conditions, only two half-channel and one rib of the cell are analyzed in 2D under the assumptions of plane strains. Figure 1 shows the geometric scheme and the boundary conditions of the MEA and BPP assembly that contains one cell stack. The material behavior of each component was assumed homogenous linear elastic (Table 2). To assemble the stack together, a clamping force imposed on the top of the End plates, is modelled with a compressive mechanical pressure P=1 MPa. The contact-friction between different stack is performed by isotropic Coulomb model with a friction coefficient assumed as μ=0.3 and assume a perfect gasket assembly contact and avoids losses. It was found in [29] that the gasket had small influence on the contact pressure distribution and the electrical resistance. Several recent numerical studies show that there is an optimal clamping pressure for

which sealing and better fuel cell performance are obtained [6, 9, 11, 53]. In this study, with a high clamping pressure the gasket between the End plate and les BPP is not been taken into account.

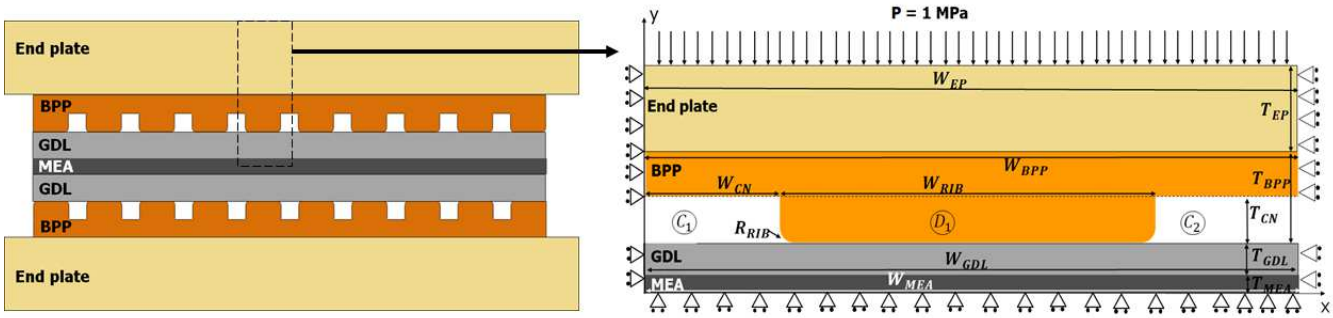

Figure 1: Geometric scheme and boundary condition of one cell stack

Table 2: Geometric dimensions and characteristics of each component of the stack

Component	Parameters	Definition	Values	Reference
End plates	T_{EP}	Thickness (mm)	5	[18]
	W_{EP}	Width (mm)	4.2	[18]
	E_{EP}	Young's modulus (GPa)	70	[18]
	ν_{EP}	Poisson's ratio	0.33	[18]
BPP	T_{BPP}	Thickness (mm)	1.5	[29]
	W_{BPP}	Width (mm)	4.2	[18]
	W_{CN}	Width of the channel (mm)	0.1	[40]
	W_{RIB}	Width of the rib (mm)	4	-
	T_{CN}	Depth of the channel (mm)	1	[29]
	R_{RIB}	Bending radius (mm)	0.04	[6]
	E_{BPP}	Young's modulus (GPa)	200	[18]
	ν_{BPP}	Poisson's ratio BPP	0.3	[18]
GDL	T_{GDL}	Thickness (mm)	0.375	[29]
	W_{GDL}	Width (mm)	4.2	[18]
	$\varnothing_P$	Diameters of the pores (mm)	0.053	[41]
	E_{GDL}	Young's modulus (GPa)	0.00613	[29]
	ν_{GDL}	Poisson's ratio GDL	0.3	[29]
MEA	T_{MEA}	Thickness (mm)	0.045	[18]
	W_{MEA}	Width (mm)	4.2	[18]
	E_{MEA}	Young's modulus (GPa)	0.021	[25]
	ν_{MEA}	Poisson's ratio	0.001	[25]

2.2 GDL porosity modelling

The microstructure of the GDL made of straight fibers corresponding to a GDL felt type (or " paper ") or curved carbon fibers (diameter varies between 5 and 10 μm) corresponding to a GDL fabric type (or "cloth") whose performance is directly related to the morphology of the carbon paper is illustrated in Figure 2. The characteristics of the pores (shape, distribution, number and dimension) and the mechanical behavior during the compression loading reduce the performance of the stack [12], [37]. The behavior of the GDL may depend on the fraction of volume occupied by the fluid phase, the size of the pores, the ratio of the size between the largest and the smallest pores, and the distance between the pores.

Investigate the effect of the porosity of GDL to obtain better cell performance by experiments seems essential. Two strategies of modelling are used to take into account the microstructure of the GDL part.

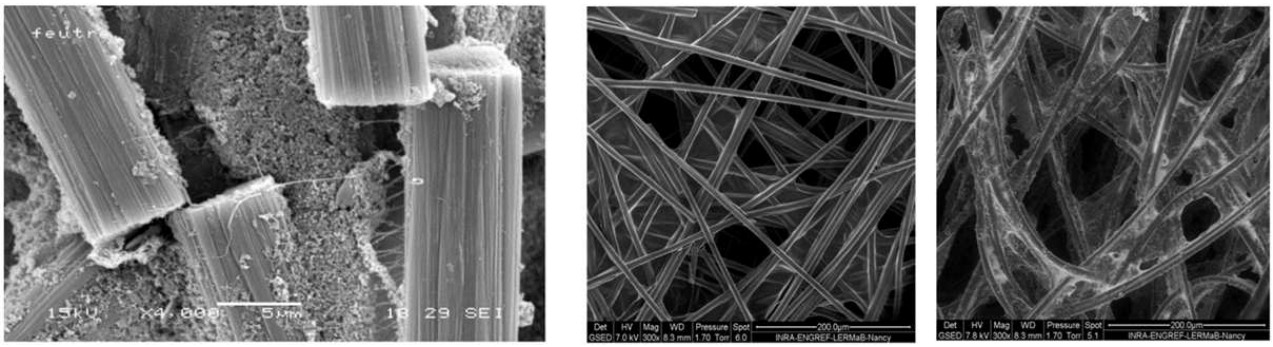

Figure 2: Morphology of the microstructure of the GDL with different pores characteristics [39]

a) Mesostructured carbon paper model

To consider the microstructure of the GDL, the pore can be modeled by periodic and random distribution using the computer-aided design accomplished using the python language script and MATLAB software [38]. In this case, the GDL is performed by spherical periodic pore distribution in which the porosity can vary from $10 \leq \varepsilon \leq 57\%$. In this 2D model, quadrilateral nonlinear finite elements with eight nodes with reduced integration (CPEG8R) are used to mesh the fuel cells component.

b) Macro homogenized model

In the macro-homogenized model, the GDL behavior is supposed as homogenous elastic material with an equivalent Young's modulus [49]. Three methods have been carried out to find the equivalent elastic properties of media:

1. *Porous GDL*: The real microstructure of porous GDL material is based on the assumption of a periodic distribution of pores. The unit cell model with repetitive pores of diameter $\varnothing_P$ is used to estimate the porosity of the GDL as $\varepsilon = \frac{m.\pi.\varnothing_p^2}{4.W_{GDL}.T_{GDL}}\%$ [29] with m is the number of pore, $\varnothing_P$ is the diameter of the pores, W_{GDL} and T_{GDL} are respectively the width and the thickness of the GDL and E_{GDL} is the elastic Young's modulus. Advantage of this technique makes it possible to take into account the real inclusions of the porous GDL but require large meshes and significant computing times.
2. *Homogenous-porous GDL*: For the EVR taken from heterogeneous material, the overall structure can be considered on a macroscopic scale as homogeneous with inclusions, which have different dimensions, positions, orientations and distributions. In this case, the porous structure of the GDL is based on the assumption of continuous media with inclusions in which the pore microstructure geometry is considered with weak elastic mechanical properties E_{pore} = 0.001MPa. Advantage of this technique makes it possible to consider the microstructural properties of the cells of porous materials of the GDL and does not require large meshes and significant computing times.
3. *Homogenous-continuum GDL*: In this case, the effective constitutive model of porous GDL is performed with the use of the homogenization technique. The technique that links the microstructure to the macroscopic scale of the material is Mori-Tanaka model [52]. The equivalent Young's modulus of the continuum homogenous GDL material E_{eq} is estimate numerically by inverse identification (variation of the contact pressure between GDL/BPP according to the GDL contact position). The homogenous elastic modulus of porous GDL is function of the GDL porosity ε and the coefficient $0 < n < 1$ as:

$$E_{eq} = E_{GDL} (1- \varepsilon)^n \qquad (1)$$

Advantage of this technique makes it possible to take into account the effective constitutive properties of porous GDL using the homogenization technique and particular for very high porosities and not require large meshes and significant computing times.

The comparison between the predicted results of these methods is illustrated in Figure 3. The graph shows the variation of the pressure between GDL/BPP according to the GDL contact position using three models. A zero contact pressure is observed under the channels corresponding to the not contact between the GDL/BPP. The contact pressure increases under the rib of the bipolar plate

and is located at the GDL detachment point, which generates peak pressure. This contact pressure is distributed almost evenly in saw teeth between C_{press}= 1.15 and 0.83 MPa. Since the structure of the GDL is composed of circular pores, the m the pressure peaks correspond to the pore positions located under the rib of the bipolar plate. We see that under the rib, there are 34 pores in the GDL, which correspond to the 34 peaks. In the homogenous-continuum model with an equivalent Young's modulus, we noting a uniform variation of the contact pressure. Under the rib of the bipolar plate, the contact pressure corresponds to the average of the peaks observed in the two other models.

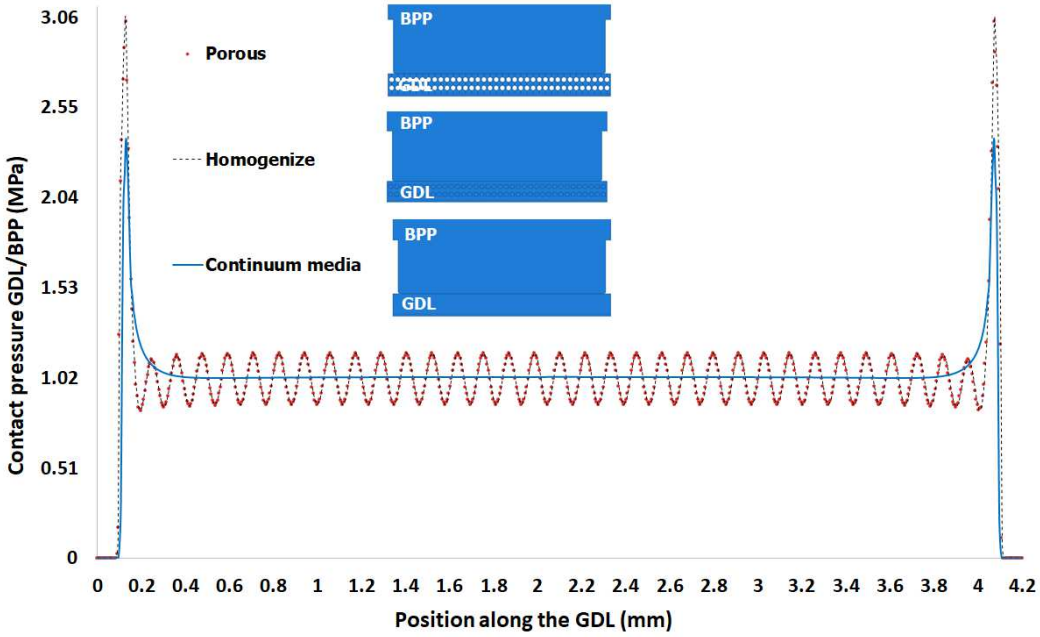

Figure 3: Inverse identification approach using different model

2.3 Contact resistance modelling

In a PEMFC, several cells composed of several stack components, are combined in series to give a high power and voltage. Among these components, the GDL and the bipolar plate are main elements and occupy more than 80% of the total mass. The mechanical contact between GDL/BPP strongly depends on the contact area, which allows the passage of the electric current thereby affecting the electrical contact resistance. The electric power lines constrict to traverse the actual contact surface, causing a decrease in the volume of material used for electrical conduction and an increase in electrical resistance.

Several studies have shown that 59% of the electrical power loss is due to the contact resistance GDL/BPP [42], [43]. This state of contact strongly depends on the external assembly clamping

force, thickness of each component, porosity and permeability of the GDL, channel width of BPP. The goal is to identify the fuel cell parameters that have the most impact on the electric conductivity of the assembly. To determine the electrical contact resistance in fuel cell two approaches have been are proposed (Figure 4).

a) Mechanical approach

In this case, the fuel cell is subject to isothermal mechanical loading (P=1MPa) to estimate the contact surface $S_{GDL/BPP}$ and the contact pressure C_{press} between the GDL/BPP. The interfacial electrical contact resistance R between the GDL/BPP is estimated analytically using the nonlinear response relationship [44]:

$$R = \frac{A}{S_{GDL/BPP}} * \left(\frac{B}{C_{press}}\right)^{\beta} \quad (2)$$

where $S_{GDL/BPP}(mm^2)$ is the contact surface between GDL/BPP, C_{press}(MPa) is the mechanical interfacial contact pressure GDL/BPP ; $A(\Omega.mm^2)$; B(MPa) and β are the interfacial electrical and mechanical coefficients of the BPP and the GDL estimate experimentally [36].

The mechanical approach is adapted to estimate indirectly the interfacial electrical resistance by determining the mechanical contact pressure distribution and the current contact surface GDL/BPP. Success in mechanical simulating forward models leads to ambitions for inverse problems, sensitivity analysis, uncertainty quantification, model-constrained optimization, and reduced-order modeling.

b) Multi-physical approach

In this case, the fuel cell is subject to mechanical loading (P=1MPa) and electrical conditions (current density $J(A/mm^2)$ at the interface GDL/BPP) to estimate directly the potential of the two sides of the interface GDL/BPP. The interfacial electrical contact resistance between the GDL/BPP is estimated using the linear response relationship:

$$R = \frac{(U_{BPP} - U_{GDL})}{J} \quad (3)$$

where $J(A/mm^2)$ is the current density at the interface GDL/BPP, $(U_{BPP} - U_{GDL})$ is the potential of the two sides of the interface.

The multi-physical approach is adapted to integrate and couple within a single software all physical phenomena in fuel cell (mechanical, electrical, thermal and chemical reaction). This

approach provides excellent results and it makes to estimate directly the interfacial electrical resistance GDL/BPP by integrating the mechanical tightening and the electrical properties of all fuel cell components.

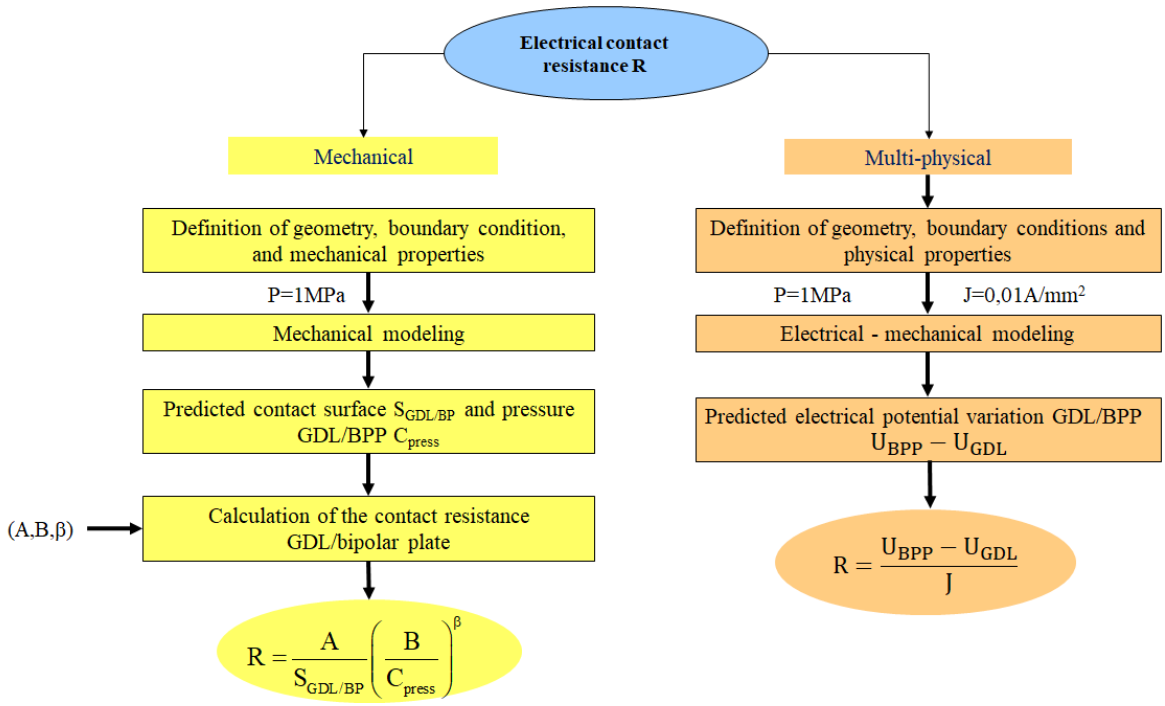

Figure 4: Mechanical and muti-physical methods of calculating the electrical contact resistance of fuel cell

3. Results and discussion

Since the GDL is the most sensitive component in the fuel cell, then its physical structure and its initial behavior change in compression. A high clamping pressure leads on the one hand, to an increase in the conductivity of the GDL and a decrease in the ohmic losses during the chemical reaction. In addition, a decrease in the porosity of the GDL leading to an insufficient circulation of reactive gases: the water produced by the electrochemical reaction wouldn`t be evacuated, which leads to a flood in the plate GDL and reduces the performance of the fuel cell. The performance of the fuel cell is enhanced by the increase of the GDL porosity, decrease of the contact resistance between GDL/BPP and the increase of the conductivity.

Thus, the variation in the conductivity and porosity of the GDL according to the clamping pressure allows us to identify the optimal value corresponding to better fuel cell efficiency. The initial porosity of the GDL varies between $60 \leq \varepsilon \leq 90\%$ and the thickness between $250 \leq T_{GDL} \leq 450\ \mu m$, however during assembly, and in order to ensure sealing, the volume of the GDL decreases from 10 to 40% therefore, the porosity decreases and the conductivity increases.

As previously mentioned, the GDL is the most sensitive to contact pressure and the porosity variation, we propose in this section, to study by design of experiments (DOE) the effect of two cases of porous GDL (low and high porosity) on the distribution of contact pressure between the GDL/MEA and the GDL/BPP. Analysis of variance and multilinear regression were performed for each DOE, in order to estimate the most influential parameters and to establish the relationship between the input and output parameters

3.1 Design of experiment DOE for a low porosity of the GDL ($10 \leq \varepsilon \leq 57\%$)

To go further in the study of contact pressure, an experimental plan has been realized, with the aim of identifying the influence existing between three types of factors. The statistical approach of the experimental design leads to a better knowledge of the system for a minimal number of tests and makes it possible to improve the mathematical modeling by optimizing the performance of the fuel cell system [45-48]. The porous GDL model is used to simulate the fuel cell assembly using DOE approach with three parameters: (parameter A) the thickness of the GDL (T_{GDL}), (parameter B) the bending radius of the bipolar plate (R_{RIB}) and (parameter C) the porosity (defined by the diameter of the pores $\varnothing_P$).

a) Design of experiment approach (DOE)

To study the electrical performance of the fuel cell and the effect of and the significance of the of the component parameters, the DOE is performed with three parameters and three modalities plan giving us 27 experiments (Figure 5).

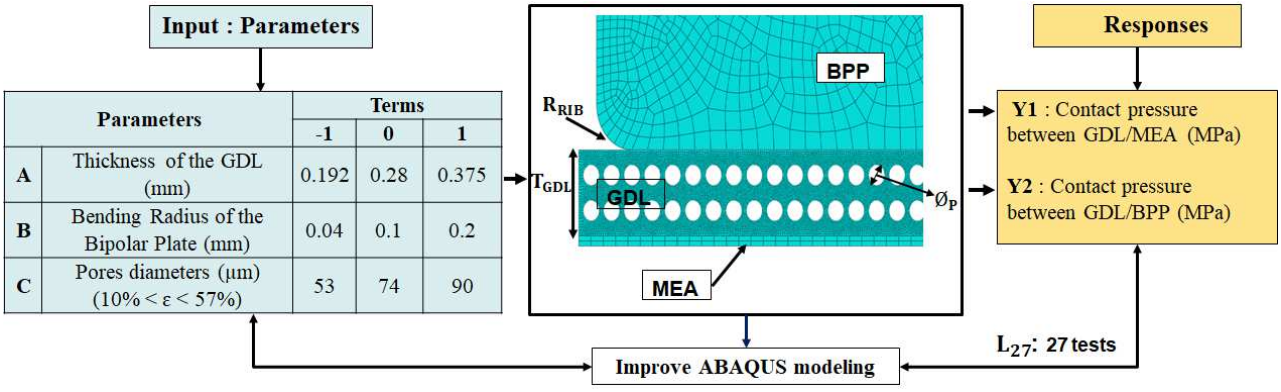

Figure 5: Modalities for different studied parameters and responses

Figures 6.a and 6.b show respectively the charts of the effects of three parameters on the contact pressure GDL/MEA and GDL/BPP. By referring to the chart of Figure 6.a, we can see a significant influence (54.36 %) of the thickness of the GDL (parameter A) on the distribution of the contact

pressure GDL/MEA. The lowest level of the thickness of the GDL tends to increase the contact pressure from C_{press} = 1.105 to 1.56 MPa (54.36%). With the increase in the contact pressure, a greater amount of water promotes the hydration of the membrane. An increase in pore diameters (from $\varnothing_p$ = 0.053 to 0.09 mm) tends to increase by 22.23 % the contact pressure GDL/MEA from C_{press} = 1.16 to 1.46 MPa. This increase in contact pressure improves the diffusion of reactive gases from the bipolar plate channels to the membrane, which avoids the phenomena of drying of the membrane and thus improve the performance of the fuel cell. A little influence was observed for the BPP bending radius parameter on the contact pressure.

For the contact GDL/BPP, Figure 6.b shows us a significant influence of the bending radius R_{BIB} on the distribution of the contact pressure. When the bending radius increases, the contact pressure between GDL/BPP decreases by 70.24% from 2.75 to 1.8 MPa (same results found and observed in [29]). The increase in the pore diameter from $\varnothing_P$ = 0.053 to 0.09 mm causes an increase of the GDL porosity of ε = 20 to 57% and the contact pressure from C_{press} = 1.987 to 2.366 MPa. A diameter of $\varnothing_P$ =0.09 mm accelerates the diffusion of the reactive gases and the evacuation of the water produced by the electrochemical reaction, thus avoiding the phenomena of flooding in the GDL plate. This increase in porosity causes a decrease in water saturation and thus an increase in the performance of the fuel cell (other studies have arrived at the same conclusion [24, 40, 50]). For a thickness T_{GDL} = 0.192 mm, the contact pressure distribution is very high (C_{press} = 2.35 MPa).

A little influence on the contact pressure was observed for the GDL thickness. Therefore, this leads to better evacuation of the liquid water and a decrease in the contact resistance between GDL/BPP and thus an improvement in the performance of the fuel cell. On the other hand, reducing the thickness of the GDL reduces the resistance to mass transport of the reactive gases. The thickness and the porosity of the GDL decrease with the clamping pressure, and as the diffusion and permeability coefficients are functions of the porosity, so these properties also decrease by the compression of the GDL.

A very high clamping force makes it possible to break the carbon fibers [14] and the occurrence of cracks, which increases the resistivity of the GDL and limits the diffusion. Hence, a relationship between thickness of the GDL, porosity and contact pressure must be defined in order to performed the optimal clamping pressure for each thickness of the GDL, thus allowing an improvement in the performance of the fuel cell. In addition to the effect graphs, analysis of variance (ANOVA) were performed for two responses: the contact pressure between GDL/MEA

(see Table 3) and GDL/BPP (see Table 4).

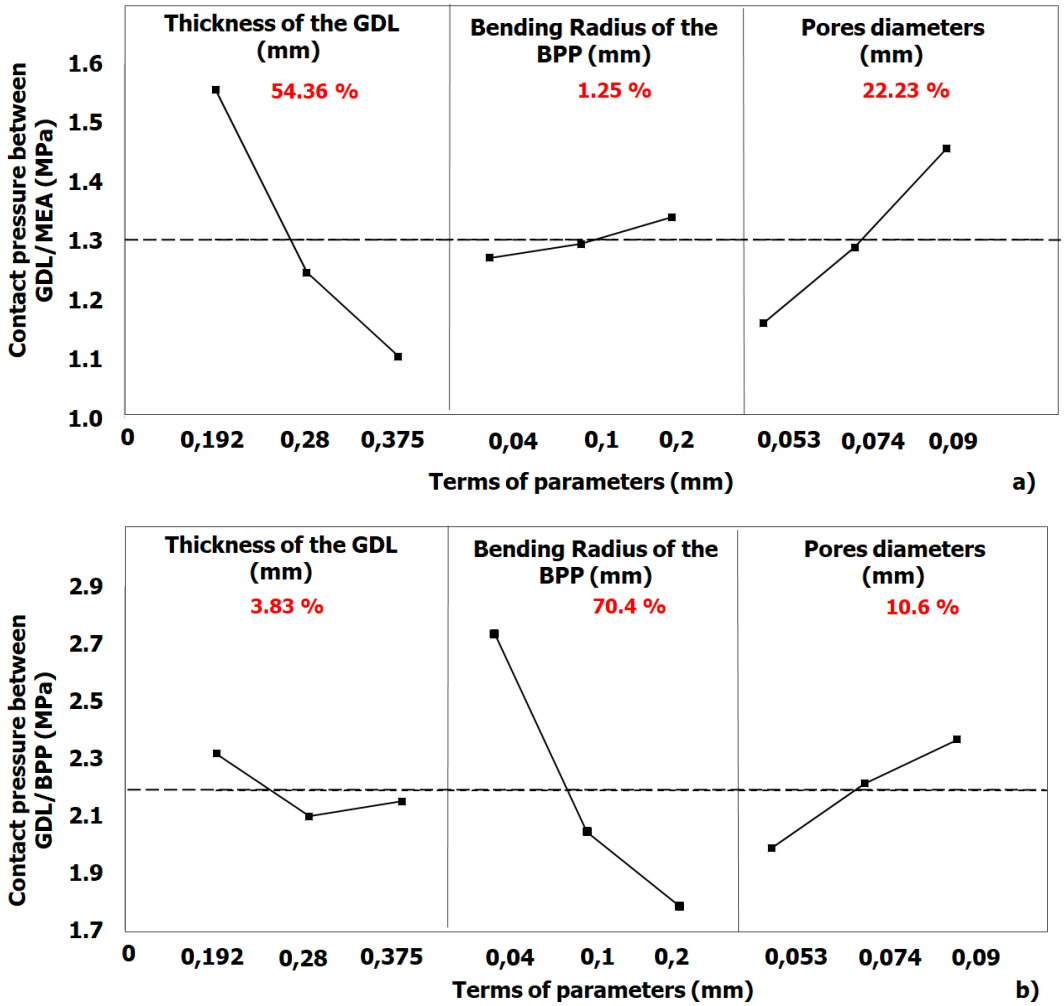

Figure 6: Chart of the effects of the three parameters on the contact pressure between: a) GDL/MEA and b) GDL/BPP.

b) Analysis of variance approach (ANOVA)

To confirm our conclusion, the next step is to analyze the values of the responses which purpose is to measure the influence of the parameters on the observed variation of the response. In order to achieve this goal, it seemed appropriate to carry out an analysis of the variance. The statistical tool "ANOVA" consists in determining from which threshold an effect can be considered as significant. In ANOVA corresponding to contact pressure GDL/MEA (Table 3), a strong interaction is observed between the two parameters A and C: an increase in the GDL pore diameter $\varnothing_p$ and a decrease in the thickness T_{GDL} cause a non-linear increase in the contact pressure

GDL/MEA. There is no interaction between the parameters AB and BC. For the contact pressure GDL/BPP (Table 4), the parameters A, B and C are the most significant. The AB and AC interactions have a strong impact; however, the BC and ABC interactions present a small effect.

Table 3: ANOVA table of contact GDL/MEA of low porosity of the GDL (S: Significant)

Parameters		Sum sq.	%	df	Mean sq.	fs	Test (fs_{theo} =3.01)
0.192 <T_{GDL} < 0.375	**A**	**9.16E-01**	**52**	**1**	**9.16E-01**	**5.64E+03**	**S**
	A^2	4.22E-02	2.4	1	4.22E-02	2.60E+02	S
0.04 < R_{RIB} < 0.2	B	2.14E-02	1.2	1	2.14E-02	1.31E+02	S
0.053 < $\varnothing_p$ < 0.09	**C**	**3.90E-01**	**22.1**	**1**	**3.90E-01**	**2.40E+03**	**S**
	A^2C	2.01E-02	1.14	1	2.01E-02	1.24E+02	S
	C^2	2.40E-03	0.14	1	2.40E-03	1.48E+01	S
	AC^2	3.38E-03	0.19	1	3.38E-03	2.08E+01	S
	AC	**3.65E-01**	**20.7**	**1**	**3.65E-01**	**2.25E+03**	**S**
	RES	2.92E-03	0.17	18	1.62E-04	-	-
	Total	1.76E+00	100	26	-	-	-

Table 4: ANOVA table of contact GDL/BPP of low porosity of the GDL

Parameters		Sum sq.	%	df	Mean sq.	fs	Test (fs_{theo} = 3.05)
0.192 <T_{GDL} < 0.375	A	1.25E-01	2	1	1.25E-01	3.39E+01	S
0.04 < R_{RIB} < 0.2	**B**	**4.07E+00**	**66**	**1**	**4.07E+00**	**1.10E+03**	**S**
	AB	1.95E-01	3.2	1	1.95E-01	5.29E+01	S
	B^2	2.78E-01	4.51	1	2.78E-01	7.55E+01	S
0.053 < $\varnothing_p$ < 0.09	**C**	**6.44E-01**	**10.5**	**1**	**6.44E-01**	**1.75E+02**	**S**
	AC	3.65E-01	5.9	1	3.65E-01	9.91E+01	S
	A^2	1.11E-01	1.8	1	1.11E-01	3.02E+01	S
	B^2C	1.15E-01	1.9	1	1.15E-01	3.12E+01	S
	ABC	1.36E-01	2.2	1	1.36E-01	3.69E+01	S
	A^2C	7.60E-02	1.23	1	7.60E-02	2.06E+01	S
	RES	5.89E-02	0.95	16	3.68E-03	-	-
	T	6.17	100	26	-	-	-

c) MultiLinear Regression approach (RML)

To model the relationships between the input parameters and the responses, and after obtaining the significant parameters for each of the two responses studied, a multilinear regression was performed. This modeling is performed to estimate the parameters of a specific model, by measuring the

dependence of the responses on the inputs of the process. Since, each parameter of Figure 5 has three modalities, which gives nonlinear effects, the simplified multilinear regression equations for the two contacts components are:

1. Contact pressure C_{press} between GDL/MEA:

$$Y_1 = 1.213 - 0.243A + 0.0315B + 0.1005C + 0.102A^2 - 0.176AC + 0.0385\,C^2 + 0.073\,A^2C + 0.0265AC^2 \quad (4)$$

2. Contact pressure C_{press} between GDL/BPP:

$$Y_2 = 2 - 0.02A - 0.4515B - 0.061C + 0.087A^2 - 0.124AB + 0.1715B^2 - 0.1818AC + 0.20575\,A^2C - 0.1304ABC + 0.2375B^2C \quad (5)$$

Figures 7 illustrated the comparison between the predicted responses and the RML results. On the level of the contact pressure response GDL/BPP (Y_2), the values of the RML model are not dispersed and remain close to the values obtained by simulation with coefficients of determination close to 1, which corresponds to a model with a very good predictive power.

The analysis of the results of the DOE shows that a better behavior of the fuel cell is observed for the modalities of the following parameters: thickness T_{GDL} = 0.192 mm, R_{RIB} = 0.04 mm and $\varnothing_P$ = 0.09 mm with a porosity of 57%. It should be noted that the pore diameter of $\varnothing_p$=0.09 mm increases the contact pressure GDL/BPP (Figure 6.b) which decreases the electrical contact resistance and improves the performance of the fuel cell. However, the choice of GDL porosity (distribution, position, orientation and shape of pores) depend on the clamping pressure P. A strong clamping pressure causes a decrease of the thickness, as well as a decrease of the diameters of the pores, which can provoke a non-linear deformation of the GDL (non-linear porosity and permeability).

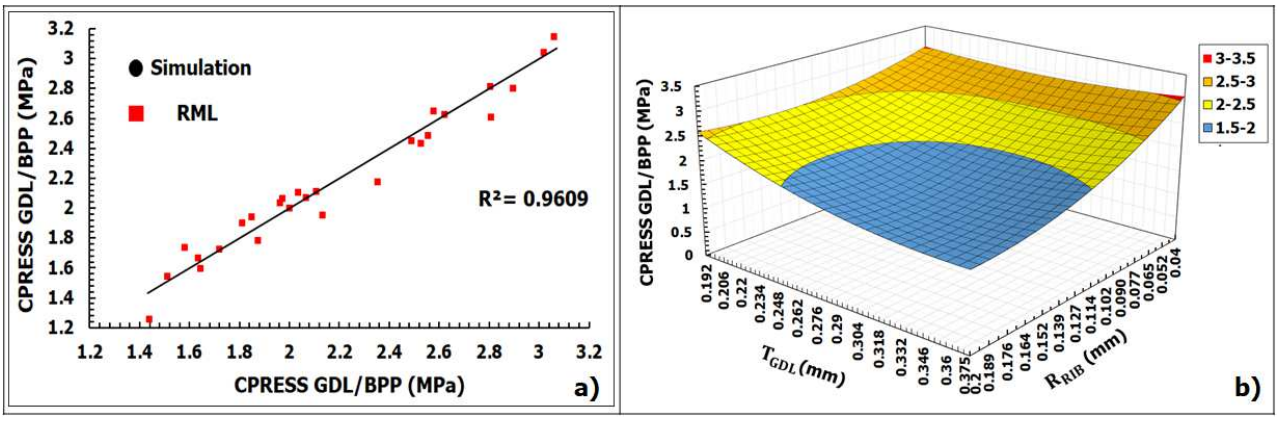

Figure 7: a) Contact pressure C_{press} between GDL/BPP and b) response surfaces for a low porosity

3.2 Design of experiment for a high porosity of the GDL ($68 < \varepsilon < 88\%$)

In this part, we will present the study of the design of experiments for a high porosity. The parameters used in the DOE are: T_{GDL}, R_{RIB} and E_{eq}. In this case, a homogenous continuum GLD model is used to predict the contact pressure GDL/MEA and GDL/BPP.

a) Design of experiment approach (DOE)

In this part, three levels of porosity are chosen (ε = 68, 78 and 88%). An experimental plan was performed as shown in Figure 8. Figures 9.a and 9.b show respectively the charts of the effects of these three parameters on the contact pressure GDL/MEA and GDL/BPP. In Figure 9.a, we can see a significant influence (an increase in the order of 86.8 %) of the parameter R_{RIB} on the distribution of the contact pressure GDL/MEA. A little influence was observed for the E_{eq} (function of the porosity and the elastic modulus the GDL material). The thickness T_{GDL} effects the contact pressure GDL/MEA with percentage around 12.18%. For the contact pressure GDL/ BPP (Figure 9.b) we observe the inverse phenomena in which 85.41% of pressure decrease is obtained with the parameter R_{RIB} and 12.34% of pressure increase is obtained with the parameter T_{GDL} (results observed also experimentally in [28]). A porosity of the GDL of 68% makes it possible to obtain a high contact pressure. A little influence was observed for the porosity (Other studies obtained at the same results [24, 40, 50, 53, 54]).

For the same width of the GDL W_{GDL} = 4.2mm and the same clamping force P = 1.0MPa, if the bending radius of the Bipolar plate increase, the contact surface with the GDL decrease which causes an increase in the contact resistance.

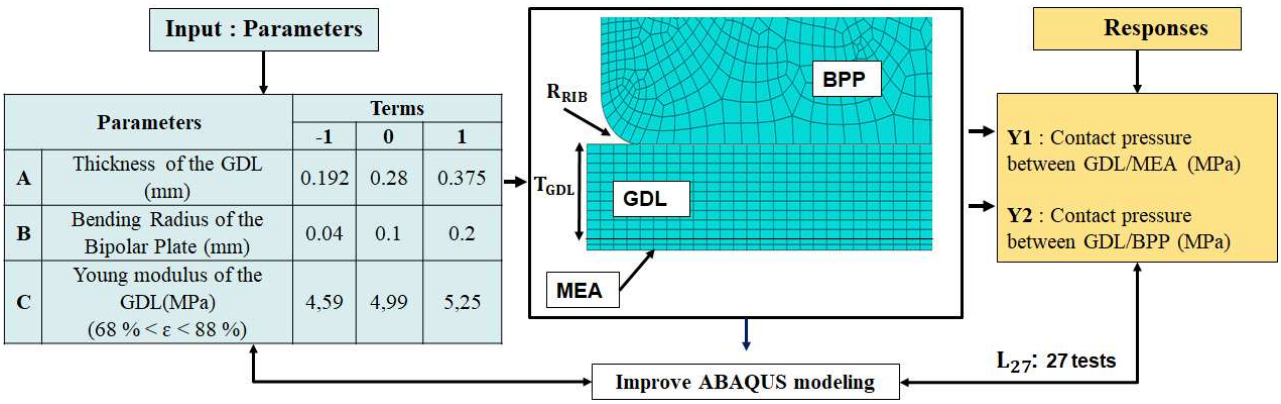

Figure 8: Modalities for Different Studied Parameters and Responses

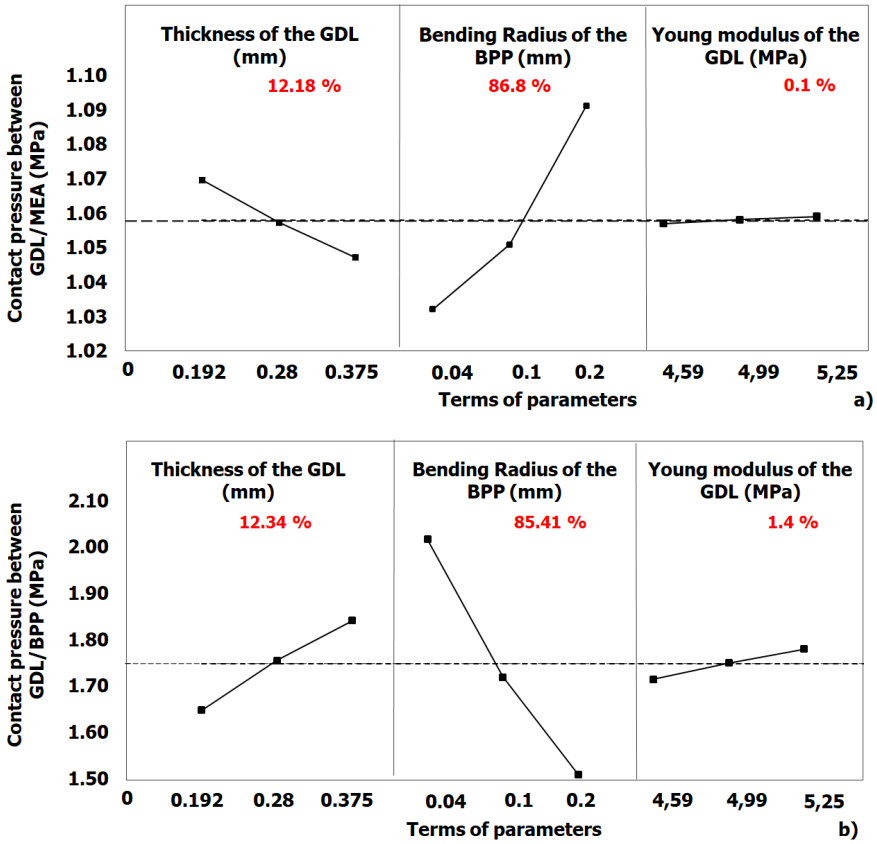

Figure 9: Chart of the effects of the three parameters on the contact pressure between: a) GDL/MEA and b) GDL/BPP.

b) Analysis of variance approach (ANOVA)

Tables 5 and 6 show respectively the results of the analysis of the variance for the two responses studied: Y_1 (contact pressure GDL/MEA), Y_2 (contact pressure GDL/BPP). In ANOVA corresponding to the contact pressure GDL/MEA, the parameters T_{GDL} and R_{RIB} appear significant. The interaction between the two parameters has a little effect. For the contact GDL/BPP, the three parameters are have significant effects on the contact pressure.

Table 5: ANOVA of contact pressure GDL/MEA of high porosity of the GDL

Parameters		Sum sq.	%	df	Mean sq.	fs	Test (fs_{theo}=2.95)
0.192 <T_{GDL} < 0.375	**A**	**2.29E-03**	**12.2**	**1**	**2.29E-03**	**1.46E+03**	**S**
0.04 < R_{RIB} < 0.2	**B**	**1.57E-02**	**83.1**	**1**	**1.57E-02**	**9.98E+03**	**S**
	B^2	6.90E-04	3.66	1	6.90E-04	4.40E+02	S
	AB	1.69E-04	0.90	1	1.69E-04	1.08E+02	S
	RES	3.45E-05	0.18	22	1.57E-06		

	T	1.88E-02	100	26			

Table 6: ANOVA of contact pressure GDL/BPP of high porosity of the GDL

Parameters		Sum sq.	%	df	Mean sq.	fs	Test (fs_{theo}=2.99)
0.192 <T_{GDL} < 0.375	**A**	**1.68E-01**	**12.3**	**1**	**1.68E-01**	**9.73E+02**	**S**
	AB^2	6.94E-03	0.51	1	6.94E-03	4.01E+01	S
0.04 < R_{RIB} < 0.2	**B**	**1.16E+00**	**84.6**	**1**	**1.16E+00**	**6.70E+03**	**S**
	B^2C	1.59E-03	0.12	1	1.59E-03	9.17E+00	S
	B^2	1.17E-02	0.85	1	1.17E-02	6.77E+01	S
	BC	6.31E-04	0.05	1	6.31E-04	3.65E+00	S
4.52 < E_{eq}< 5.25MPa 68 % < ε < 88%	**C**	**1.91E-02**	**1.40**	**1**	**1.91E-02**	**1.11E+02**	**S**
	RES	3.29E-03	0.24	19	1.73E-04		
	T	1.37	100	26			

- *Multilinear regression approach (RML)*

The simplified multilinear regression equations for each contact GDL/MEA and GDL/BPP are defined as:

1. Contact pressure between GDL/MEA:

$$Y_1 = 1.05 - 0.0105A + 0.03B - 0.004AB + 0.011B^2 \quad (6)$$

2. Contact pressure between GDL/BPP:

$$Y_2 = 1.737 + 0.124A - 0.249B + 0.0205C + 0.021B^2 - 0.046AB^2 - 0.0113BC + 0.02425B^2C \quad (7)$$

Figures 10 illustrated the comparison between the predicted responses and the multilinear regression results. On the level of the response Y_2, the values of the RML model are not dispersed and remain close to the values obtained by simulation with coefficients of determination close to 1, which corresponds to a model with a very good predictive power. To visualize the combined effect of these parameters, the response surfaces and contour plots were generated for each parameter of the fitted models. Figures 10 the effect of T_{GDL} and R_{RIB} on contact pressure GDL/BPP. We note that, the maximum response GDL/BPP occurs when the thickness of the GDL is at his highest level and the bending radius of the bipolar plate is at the lowest level.

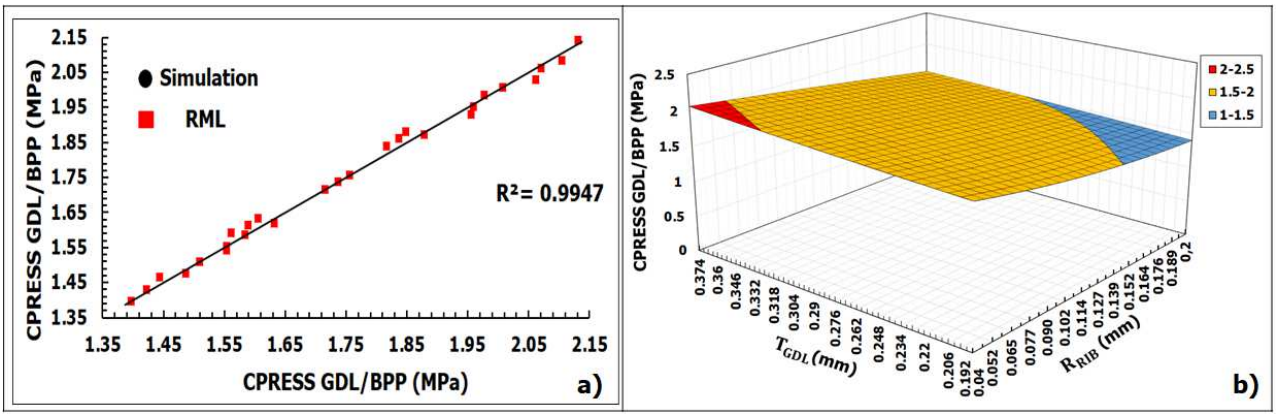

Figure 10: a) Contact pressure between GDL/BPP and b) response surfaces for a high porosity

3.3 Optimized fuel cell stack

The experimental study gives us the choice of the optimal parameters corresponding to a better behavior of the fuel cell stack: the thickness of the GDL is T_{GDL} = 0.375 mm, the bending radius of the bipolar plate is R_{RIB} = 0.04 mm and the GDL equivalent Young's modulus is E_{eq} = 4.59MPa with the porosity of ε= 88%. Under the applied assembly pressure P = 1MPa, the predicted results show the distribution of equivalent von-Mises stress for the GDL and BPP at the corresponding surface and the contact pressure (Figure 11.a). The von-Mises stress at the interface of the GDL and the BPP is estimated at 0.99 MPa and the maximum value around of 3.67 MPa is localized in the corner radius of the BPP. The maximum pressure is located at the GDL detachment point from the bipolar plate, which generates peak pressures at the detachment point.

The contact pressure between GDL/MEA and GDL/BPP is distributed uniformly (C_{press}= 1.02 MPa) in the area between the rib of the bipolar plate (see Figure 11.b). Under the BPP channel where a swelling of the GDL appears, which causes a separation between the GDL and MEA with a contact pressure which tends towards zero.

However, since the width of the channel is very small (0.1mm), there was not a complete separation between GDL and MEA and the contact pressure GDL/MEA decreases to reach a minimum value under the channel (0.8 MPa).

Figure 11.c illustrates the variation of the contact resistivity GDL/BPP in accordance with the GDL contact position. We can noting that the electrical resistivity per unit surface of the fuel cell stack R= 82.4 $10^{-3}\Omega$.

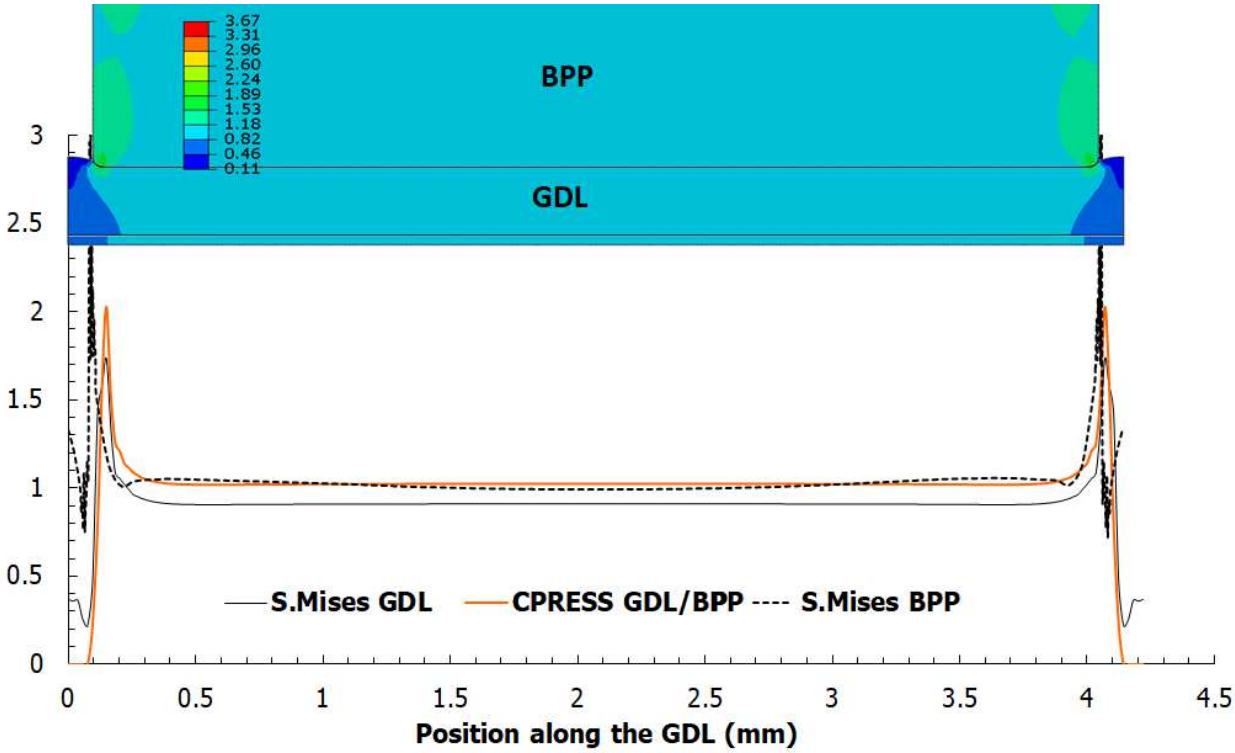

Figure 11.a: Distribution of von-Mises stress and the contact pressure along the GDL line (P=MPa)

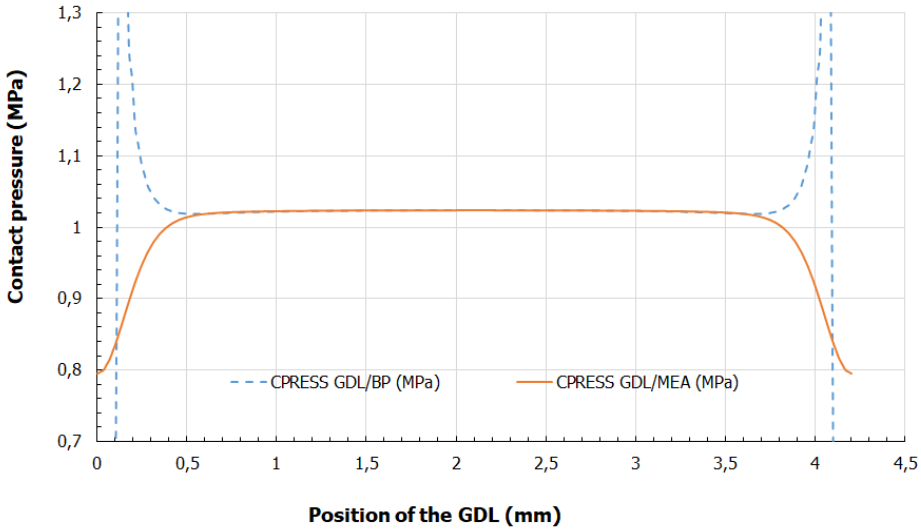

Figure 11.b: Distribution of the contact pressure between GDL/BPP and GDL/MEA all along the GDL line.

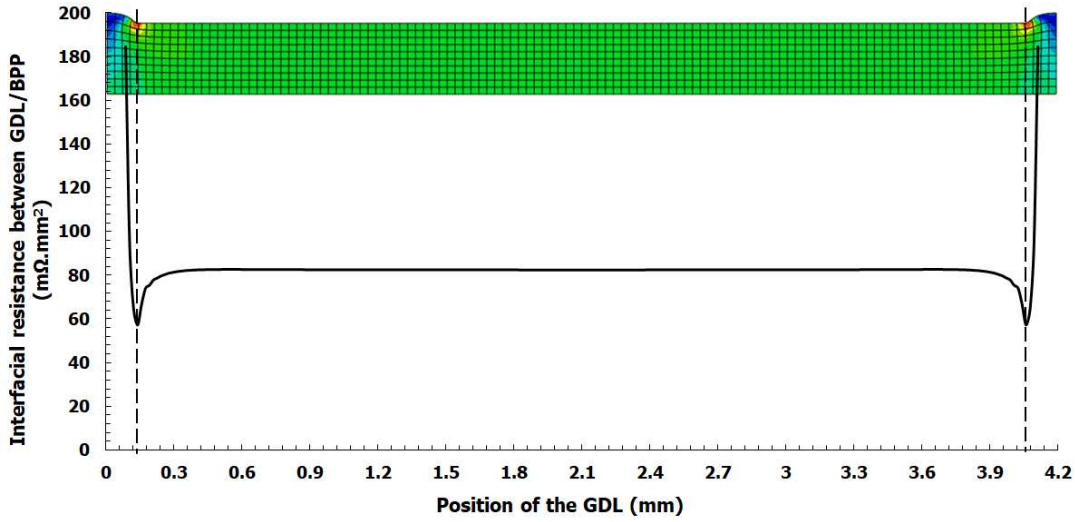

Figure 11.c: Interfacial electrical resistance between GDL/BPP along the GDL line (P=1 MPa)

To study the effect of the clamping assembly pressure on the electrical contact resistance of PEMFC, a series simulation is performed with a range of P from 0.3 to 1.5 MPa. For each clamping pressure, an average value of the contact resistance GDL/BPP is obtained. Under a compression of P=1.0MPa, the contact pressure between GDL/BPP as a function of the position of the GDL is illustrated in Figure 11.b. By using Eq. 2, we calculate the different values of the contact resistance (R) for each value of the contact pressure C_{press} between GDL/BPP of the area located under the rib of the bipolar plate. Then, an average value of the contact resistance is estimated. Mishra, V. *et al.* [36] experimentally studied the effects of different gas diffusion layer and clamping pressure for six types of GDL (GDL -10BA, GDL -10BB, B-3/2050, B-2/120, B -1 / B and B-1 / D). A fractal asperity based model is adopted to predict the contact resistance as a function of pressure, material properties, and surface geometry.

Knowing the contact pressure C_{press} evolution along the interfacial surface contact GDL/BPP (see the figure below) we estimate the electrical resistance R using the average mechanical contact pressure C_{press} for the clamping pressure P = 1 MPa: A= 3.32 10^{-3} Ωcm^2; B= 1.01MPa and β=0.534. The electrical resistance is :

$$R_{Sim} = 3.32 * \left(\frac{1.01}{1.02}\right)^{0.534} = 3.29 \text{m}\Omega\text{cm}^2$$

A comparison of predicted contact resistance versus clamping pressure with experimental values of reference [36] is done in Figure 12. Good agreement between the predicted results and the experimental values. We can see that, the contact resistance decreases according the equation (8)

when the clamping pressure increases. This reduction in contact resistance leads to a reduction in ohmic losses during the chemical reaction and accelerates the diffusion of the reactive gases and the evacuation of the water produced by the electrochemical reaction, thus avoiding the phenomena of flooding in the GDL plate. To find the relationship between the electrical contact resistance and the clamping pressure P, the contact resistance R (mΩ.cm²) data is adjusted to the inverse power law as:

$$R = \frac{K}{P^{\alpha}} \tag{8}$$

Where the two constants are deduced from the trend line of numerical results K = 3.2973 and α = 0.532.

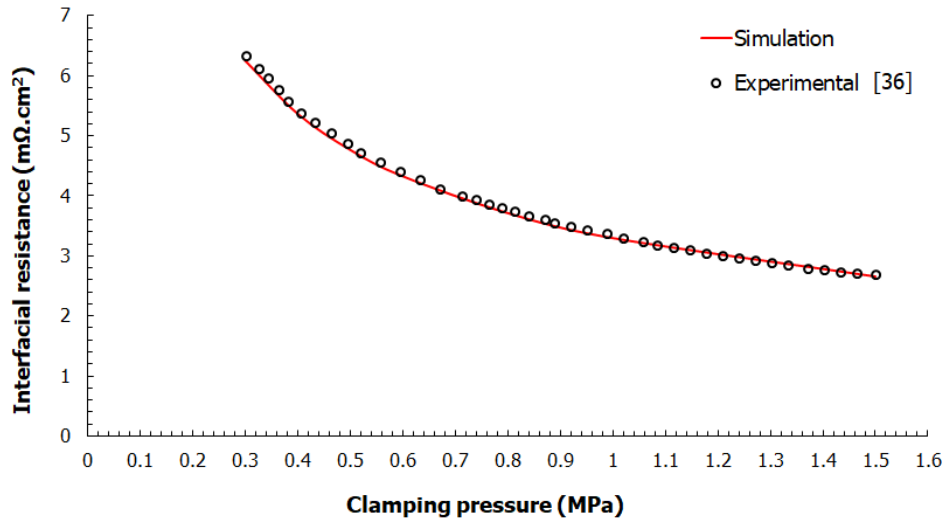

Figure 12: Electrical resistance versus clamping pressure comparison predicted model and experimental results [36]

4. Conclusion

In this study, finite element analysis is associated with a DOE to study the influence of different parameters on the mechanical behavior of the fuel cell and in particular on the contact pressures between the different components.

Our results led to the following main conclusions: The maximum contact pressure is located at the level the detaching point of the GDL from the bipolar plate, which generates pressure peaks at the detaching point.

The influence of the porosity of the GDL has also been investigated. To establish a comparison and to have a good knowledge of the phenomena, low porosity and high porosity have been

studied.

The study of the low porosity allows us to identify the optimal parameters: thickness of GDL of 0.192 mm, pore diameters of 0.09 mm and a bending radius of the bipolar plate of 0.04mm. The contact pressures between the three components of the cell (GDL/BPP and GDL/MEA) are strongly influenced by these parameters.

The increase in pore diameter ($Ø_P$ = 0.09 mm), corresponding to a porosity of 57%, with a small thickness of the GDL (0.192mm) leads to an increase in contact pressures which reduces the electrical contact resistance, avoids the drying of the membrane. Whereas a greater amount of water promotes hydration of the membrane and enhances the performance of the fuel cell. However, we didn't compare our result with experimental results because not a lot of experiments have been conducted on the study for low porosity of the GDL.

In addition, our simulations were performed under a clamping pressure of 1MPa. And as the porosity and the thickness of the GDL depends on the clamping pressure: a strong clamping pressure leads to a decrease in the thickness of the GDL and the pore diameters (closed pores), which causes a non-linear deformation in the GDL. It would be interesting, in the next future, to study, for each thickness of the GDL, the influence of compression on the distribution of contact pressures and the porosity of the GDL.

Then, a high porosity study was performed, where the geometry of the GDL with pore was replaced by a homogenized model. With the optimal parameters identified (porosity 88%, bending radius of the bipolar plate of 0.04mm and thickness of the GDL of 0.375mm), we found a good correlation between the numerical results and the experimental results found in the bibliography. This point validates our numerical model and its hypothesis.

References

[1] Chupin, S. (2009). Comportement local et performances électriques d'une pile à combustible à membrane : vers un outil de diagnostic (Thèse de doctorat, Université du Québec à Trois-Rivières, Canada).

[2] Charon, W., Iltchev, M. C., & Blachot, J. F. (2014). Mechanical simulation of a Proton Exchange Membrane Fuel Cell stack using representative elementary volumes of stamped metallic bipolar plates. *International Journal of Hydrogen Energy*, *39* (25), 13195- 13205.

[3] Vion-Dury, B. (2011). Mécanismes de vieillissement des électro-catalyseurs de pile à combustible de type PEMFC (Thèse de doctorat, Université de Grenoble, France).

[4] Coulon, R. (2012). Modélisation de la dégradation chimique de membranes dans les piles à combustibles à membrane électrolyte polymère (Thèse de doctorat, Université de Grenoble, France).

[5] Dafalla, A. M., & Jiang, F. (2018). Stresses and their impacts on proton exchange membrane fuel cells: A review. *International Journal of Hydrogen Energy*, *43* (4), 2327-2348.

[6] Akiki, T. (2011). Modélisation de la dégradation de la production de puissance d'une pile à combustible suite aux sollicitations mécaniques (Thèse de doctorat, Belfort-Montbéliard).

[7] Muthukumar, M., Karthikeyan, P., Vairavel, M., Loganathan, C., Praveenkumar, S., & Kumar, A. S. (2014). Numerical studies on pem fuel cell with different landing to channel width of flow channel. *Procedia Engineering*, 97, 1534-1542.

[8] Kahveci, E. E., & Taymaz, I. (2015). Effect of humidification of the reactant gases in the proton exchange membrane fuel cell. *J Clean Energy Technol*, 3 (5), 356-359.

[9] Lai, X., Peng, L., & Ni, J. (2008). A mechanical–electrical finite element method model for predicting contact resistance between bipolar plate and gas diffusion layer in PEM fuel cells. *Journal of Power Sources*, 182 (1), 153-159.

[10] Dey, T., Deshpande, J., Singdeo, D., & Ghosh, P. C. (2019). Study of PEM Fuel Cell End Plate Design by Structural Analysis Based on Contact Pressure. *Journal of Energy*, *2019*, Article ID 3821082, 11 pages.

[11] Movahedi, M., Ramiar, A., & Ranjber, A. A. (2018). 3D numerical investigation of clamping pressure effect on the performance of proton exchange membrane fuel cell with interdigitated flow field. *Energy*, 142, 617-632.

[12] Mason, T. J., Millichamp, J., Shearing, P. R., & Brett, D. J. (2013). A study of the effect of compression on the performance of polymer electrolyte fuel cells using electro- chemical impedance spectroscopy and dimensional change analysis. *International journal of hydrogen energy*, 38 (18), 7414-7422.

[13] Habibnia, M., Shakeri, M., & Nourouzi, S. (2016). Determination of the effective parameters on the fuel cell efficiency, based on sealing behavior of the system. *International Journal of Hydrogen Energy*, 41(40), 18147-18156.

[14] Irmscher, P., Qui, D., Janßen, H., Lehnert, W., & Stolten, D. (2019). Impact of gas

diffusion layer mechanics on PEM fuel cell performance. *International Journal of Hydrogen Energy*, 44 (41), 23406-23415.

[15] Carral, C., & Mele, P. (2014). A numerical analysis of PEMFC stack assembly through a 3D finite element model. *International journal of hydrogen energy*, 39 (9), 4516-4530.

[16] Bates, A., Mukherjee, S., Hwang, S., Lee, S. C., Kwon, O., Choi, G. H., & Park,S. (2013). Simulation and experimental analysis of the clamping pressure distribution in a PEM fuel cell stack. *International journal of hydrogen energy*, 38 (15), 6481-6493.

[17] Zhou, P., Lin, P., Wu, C. W., & Li, Z. (2011). Effect of nonuniformity of the contact pressure distribution on the electrical contact resistance in proton exchange membrane fuel cells. *International journal of hydrogen energy*, 36 (10), 6039-6044.

[18] Alizadeh, E., Barzegari, M. M., Momenifar, M., Ghadimi, M., & Saadat, S. H. M. (2016). Investigation of contact pressure distribution over the active area of PEM fuel cell stack. *International Journal of Hydrogen Energy*, 41 (4), 3062-3071.

[19] Lai, X., Ni, J., Peng, L., Lan, S., & Lin, Z. (2007). Robust design of assembly parameters on membrane electrode assembly pressure distribution. *Journal of Power Sources*, *172*(2), 760-767.

[20] Atyabi, S. A., Afshari, E., Wongwises, S., Yan, W. M., Hadjadj, A., & Shadloo, M. S. (2019). Effects of assembly pressure on PEM fuel cell performance by taking into accounts electrical and thermal contact resistances. *Energy*, *179*, 490-501.

[21] Chien, C. H., Hu, Y. L., Su, T. H., Liu, H. T., Wang, C. T., Yang, P. F., & Lu, Y. X. (2016). Effects of bolt pre-loading variations on performance of GDL in a bolted PEMFC by 3-D FEM analysis. *Energy*, *113*, 1174-1187.

[22] García-Salaberri, P. A., Vera, M., & Zaera, R. (2011). Nonlinear orthotropic model of the inhomogeneous assembly compression of PEM fuel cell gas diffusion layers. *International Journal of Hydrogen Energy*, *36*(18), 11856-11870.

[23] García-Salaberri, P. A., & Vera, M. (2015). On the effects of assembly compression on the performance of liquid-feed DMFCs under methanol-limiting conditions: A 2D numerical study. *Journal of Power Sources*, *285*, 543-558.

[24] Carcadea, E., Varlam, M., Ismail, M., Ingham, D. B., Marinoiu, A., Raceanu, M., & Ion-Ebrasu, D. (2019). PEM fuel cell performance improvement through numerical optimization of the parameters of the porous layers. *International Journal of Hydrogen Energy*, https://doi.org/10.1016/j.ijhydene.2019.08.219

[25] Vlahinos, A., Kelly, K., D'Aleo, J., & Stathopoulos, J. (2003, January). Effect of material and manufacturing variations on membrane electrode assembly pressure distribution. In *ASME 2003 1st International Conference on Fuel Cell Science, Engineering and Technology.* American Society of Mechanical Engineers Digital Collection, 2003. 111-120.

[26] Toghyani, S., Nafchi, F. M., Afshari, E., Hasanpour, K., Baniasadi, E., & Atyabi,S. A. (2018). Thermal and electrochemical performance analysis of a proton exchange membrane fuel cell under assembly pressure on gas diffusion layer. *International Journal of Hydrogen Energy*, 43 (9), 4534-4545.

[27] Zhang, L., Liu, Y., Song, H., Wang, S., Zhou, Y., & Hu, S. J. (2006). Estimation of contact resistance in proton exchange membrane fuel cells. *Journal of Power Sources*, 162 (2), 1165-1171.

[28] Bouziane, K., Lachat, R., Meyer, Y., Candusso, D., & Francois, X. (2018, July). Etude expérimentale de l'influence de la compression mécanique d'une couche de diffusion de gaz sur la résistance électrique de contact dans une pile à combustible à membrane échangeuse de protons. SYMPOSIUM DE GENIE ELECTRIQUE (SGE 2018), NANCY, France.

[29] Zhang, Z. (2010). Modélisation mécanique des interfaces multi-contacts dans une pile à combustible (Thèse de doctorat, Université de Evry-Val d'Essonne, France).

[30] Hassan, N., Kilic, M., Okumus, E., Tunaboylu, B., & Murat Soydan, A. (2016). Experimental determination of optimal clamping torque for AB-PEM fuel cell. *Journal of Electrochemical Science and Engineering*, 6 (1), 9-16.

[31] Mason, T. J., Millichamp, J., Neville, T. P., El-kharouf, A., Pollet, B. G., & Brett,D. J. (2012). Effect of clamping pressure on ohmic resistance and compression of gas diffusion layers for polymer electrolyte fuel cells. *Journal of Power Sources*, 219, 52-59.

[32] El-Kharouf, A. (2014). Understanding GDL properties and performance in polymer electrolyte fuel cells (Thèse de doctorat, University of Birmingham).

[33] Ye, D., Gauthier, E., Benziger, J. B., & Pan, M. (2014). Bulk and contact resistances of gas diffusion layers in proton exchange membrane fuel cells. *Journal of Power Sources*, 256, 449-456.

[34] Miyazawa, A., Himeno, T., & Nishikata, A. (2012). Electrical properties of bipolar plate and gas diffusion layer in PEFC. *Journal of Power Sources*, 220, 199-204.

[35] El Oualid, S., Lachat, R., Candusso, D., & Meyer, Y. (2017). Characterization process to

measure the electrical contact resistance of Gas Diffusion Layers under mechanical static compressive loads. *International Journal of Hydrogen Energy*, 42 (37), 23920-23931.

[36] Mishra, V., Yang, F., & Pitchumani, R. (2004). Measurement and prediction of electrical contact resistance between gas diffusion layers and bipolar plate for applications to PEM fuel cells. *Journal of Electrochemical Energy Conversion and Storage*, *1* (1), 2-9.

[37] El-Kharouf, A., Mason, T. J., Brett, D. J., & Pollet, B. G. (2012). Ex-situ characterization of gas diffusion layers for proton exchange membrane fuel cells. *Journal of Power sources*, *218*, 393-404.

[38] Zhu, S., Bouby, C., Cherouat, A., & Zineb, T. B. (2019). 3D reconstitution and numerical analysis of superelastic behavior of porous shape memory alloy. *International Journal of Solids and Structures,* 168, 109-122.

[39] Bouziane, K., Zamel, N., Francois, X., Meyer, Y., & Candusso, D. (2019). Effects of mechanical compression on the performance of Polymer Electrolyte Fuel Cells and analysis through in-situ characterisation techniques-A review. *Journal of Power Sources*, *424*, 8-26.

[40] Jourdani, M. (2019). Simulation Numérique Couplée des Phénomènes Thermo- fluide, Electrochimique et Mécanique dans une Pile à Combustible type PEMFC (Thèse de doctorat, Ecole Mohammadia d'Ingénieurs, Maroc)

[41] Thomas, A. (2012). Transferts d'eau et de chaleur dans une pile à combustible à membrane : mise en évidence expérimentale du couplage et analyse des mécanismes (Thèse de doctorat, Université de Lorraine, France).

[42] Hamour, M., Grandidier, J. C., Ouibrahim, A., & Martemianov, S. (2015). Electrical conductivity of PEMFC under loading. *Journal of Power Sources*, *289*, 160-167.

[43] Avasarala, B., & Haldar, P. (2009). Effect of surface roughness of composite bipolar plates on the contact resistance of a proton exchange membrane fuel cell. *Journal of Power Sources*, *188* (1), 225-229.

[44] Zhou, P., Wu, C. W., & Ma, G. J. (2006). Contact resistance prediction and structure optimization of bipolar plates. *Journal of Power Sources*, *159* (2), 1115-1122.

[45] Pillet, M. (2000). Les plans d'expériences par la méthode Taguchi (p. 250).

[46] Goupy, J. (1988). La méthode des plans d'expériences : optimisation du choix des essais et de l'interprétation des résultats. Dunod.

[47] Wahdame, B. (2006). Analyse et optimisation du fonctionnement de piles à combustible par la méthode des plans d'expériences (Thèse de doctorat, Belfort-Montbeliard, France).

[48] Placca, L. (2010). Impact des incertitudes sur le fonctionnement des piles à combustible par approche fiabiliste (Thèse de doctorat, Belfort-Montbeliard, France).

[49] Lafhaj, Z., Goueygou, M., Djerbi, A., & Kaczmarek, M. (2006). Correlation between porosity, permeability and ultrasonic parameters of mortar with variable water/cement ratio and water content. *Cement and Concrete Research*, *36* (4), 625-633.

[50] Larbi, B., Alimi, W., Chouikh, R., & Guizani, A. (2013). Effect of porosity and pressure on the PEM fuel cell performance. *International journal of hydrogen energy*, 38 (20), 8542-8549.

[51] Hibbit, Karlson, Inc. S., « Abaqus », Theory Manual - version 6.5, 2005.

[52] Mori T. and Tanaka K. (1973). Average stress in matrix and average elastic energy of materials with misfitting inclusions. *Acta Metallurgica*, 21 (5), 571-574.

[53] Kahveci, E. E., & Taymaz, I. (2014). An Investigation of GDL Porosity on PEM Fuel Cell Performance. *Chemical Engineering Transactions*, *42*, 37-42.

[54] Taymaz, I., & Benli, M. (2010). Numerical study of assembly pressure effect on the performance of proton exchange membrane fuel cell. *Energy*, *35*(5), 2134-2140.

Nomenclature

T_{EP} Thickness of the End Plates (mm)

W_{EP} Width of the End Plates (mm)

E_{EP} Young's modulus of the End Plates (GPa)

ν_{EP} Poisson's ratio of the End Plates

T_{BPP} Thickness of the bipolar plates (mm)

W_{BPP} Width of the bipolar plates (mm)

W_{CN} Width of the channel of the bipolar plates (mm)

W_{RIB} Width of the rib of the bipolar plates (mm)

T_{CN} Depth of the channel of the bipolar plates (mm)

R_{RIB} Bending radius of the bipolar plates (mm)

E_{BPP} Young's modulus of the bipolar plates (GPa)

ν_{BPP} Poisson's ratio of the bipolar plates

T_{GDL} Thickness of the GDL (mm)

W_{GDL} Width of the GDL (mm)

$\varnothing_P$ Diameters of the pores of the GDL (mm)

E_{GDL} Young's modulus of the GDL (GPa)

ν_{GDL} Poisson's ratio of the GDL

T_{MEA} Thickness of the MEA (mm)

W_{MEA} Width of the MEA (mm)

E_{MEA} Young's modulus of the MEA (GPa)

ν_{MEA} Poisson's ratio of the MEA

P Clamping pressure [MPa]

ε Porosity of the GDL

m Number of pore

R Interfacial electrical contact resistance between the GDL/BPP [mΩ.mm^2]

$S_{GDL/BP}$ Contact surface between GDL/BPP [mm^2]

C_{press} Contact pressure [MPA]

A (Ω.mm^2), B (MPa) and β interfacial electrical and mechanical coefficients of the BPP and the GDL estimate experimentally [36].

J Current density at the interface GDL/BPP [A/mm^2]

U_{BPP} Electrical potential on the surface of BPP [mV]

U_{GDL} Electrical potential on the surface of GDL [mV]

Y1 Contact pressure between GDL/MEA [MPa]

Y2 Contact pressure between GDL/BPP [MPa]

Table List

Figure Captions

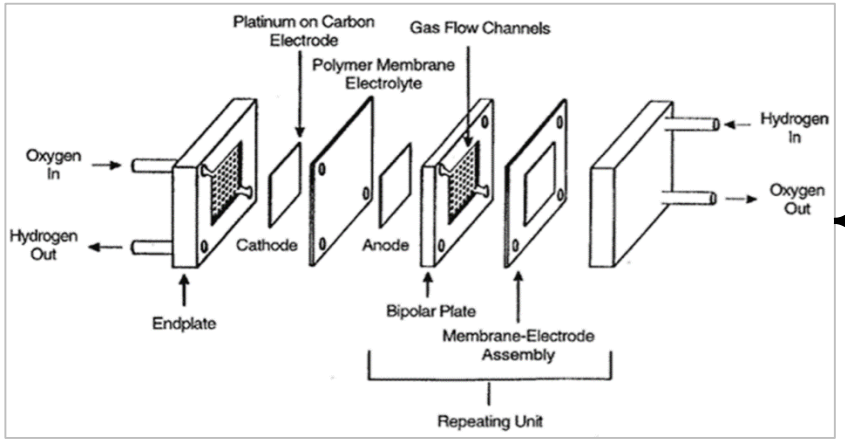

Aim: to study the effect of the porosity on the fuel cell electrical reliability.

Numerical Mechanical Model

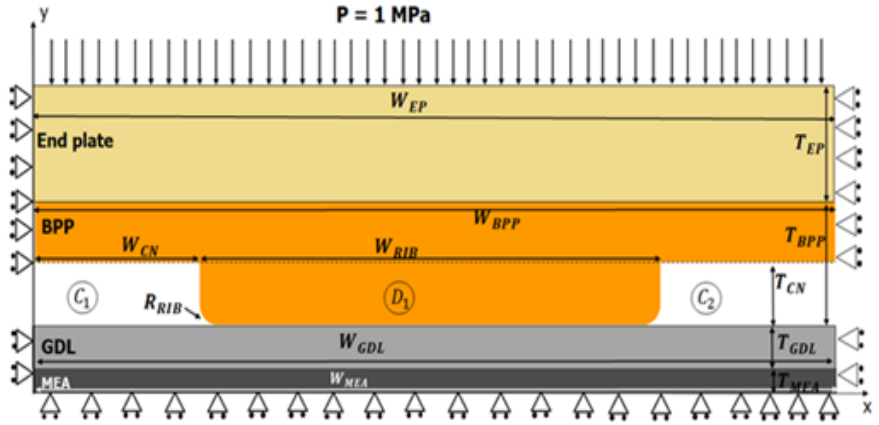

Design of experiment

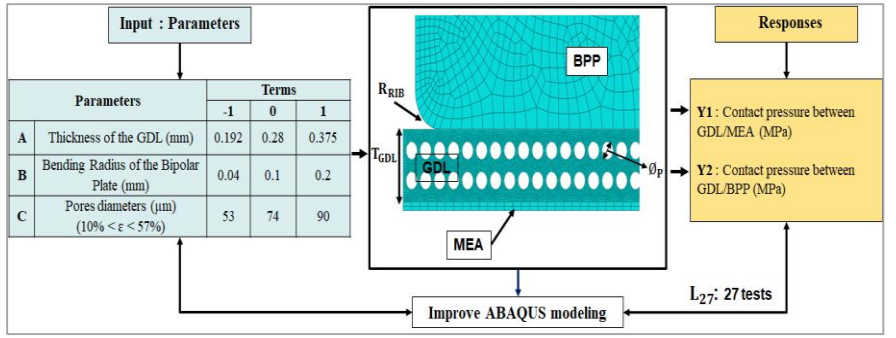

Combined effect of mechanical parameters on contact pressure between GDL/BP